

Design and development of pressure sensor based on Fiber Bragg Grating (FBG) for ocean applications

**V. V. S. Ch. Swamy¹, Saidi Reddy Parne¹, Sanjjev Afzulpurkar², Shivanand Prabhudesai²,
Vijeesh V. P.¹**

National Institute of Technology Goa¹
National Institute of Oceanography Goa²

Abstract:

A Fiber Bragg Grating (FBG) based sensors has been designed, fabricated and is being prototyped to measure the ocean water column pressure. To measure the pressure variation, a compact design is made by using stainless steel disks and rubber "O" rings in a closed air cavity setup. The pressure in static freshwater column ranging from 0 to 0.04 MPa was gauged, using closed air cavity setup. Also, another "T" shaped design, for testing, has been made of solid stainless-steel tube with the open-air cavity for an extended range of pressure sensing. By using an oil pressure pump and open-air cavity setup, pressure values from 0 to 0.5 MPa have been measured. In both setups same thickness of copper, stainless steel diaphragms are used to measure the pressure. Range of measurements has been carried out to test both the setups. Results indicate that the pressure sensitivity in closed air cavity setup is 24.95 nm/MPa with linearity 99.72%. In the open-air cavity, setup is 16.22 nm/MPa with linearity 99.34% is achieved. Simulation and experimental studies are performed to validate the efficacy of the designed FBG pressure sensor.

Introduction:

Water column pressure is a fundamental oceanography requirement towards obtaining data related to Bio-geo-chemical parameters [1]. Current pressure sensors, adequate for all basic measurements, have limitations such as low response rate, operating frequency (Hz), possible electromagnetic interference with surroundings that can cause electrical circuit damages which restrict their applications in harsh environments [2]. Optical sensors have many advantages over conventional pressure sensors which are light weight, robust, small in size, anti-corrosive, anti-electromagnetic, very fast response time, high accuracy [3,4]. Fiber optic pressure sensor mechanisms are divided into four categories based on modulation of frequency, phase modulation, modulation of wavelength, and modulation of polarization [5-7]. Out of these, wavelength modulation is simpler to interpret data, has lower cost and can detect signals from multiplexed sensors [24]. With these advantages, Fiber Bragg Grating (FBG) based sensors can be used effectively for oceanic applications [8 -10].

Juncheng et al. developed an epoxy free high temperature fiber optic pressure sensor [11]. They made a sensor head with fused silica resulting in low temperature dependence and higher operating temperature (700°C). Allwood et al. proposed high sensitive fiber Bragg grating pressure transducer with reported sensitivity of 0.116 nm/Kpa [12]. They also reported a low-cost edge filter interrogation technique instead of high cost solid state interrogators. To improve pressure sensitivity and reduce temperature effect on pressure measurement, Frantisek et al. proposed a pressure sensor based on lateral deformation of FBG and membrane deformation [13]. Here, the applied pressure range is from 0-2 bar only and peak measurement requires high resolution 10 pm, precise spectrum analyser. However standard bare FBG pressure sensitivity is 0.00304 nm/Mpa, which is much lower for practical sensing applications and due to fragile nature of FBG, some packaging technology has been required to improve the sensitivity [13]. Jun Huang et al. developed and tested a diaphragm type FBG pressure sensor with temperature compensation in the region of 0-1 Mpa [14]. They showed that their sensor sensitivity is 1.57 pm/Kpa with less hysteresis. However, while increasing the pressure sensitivity, higher temperature cross-sensitivity could not be avoided. To address this problem, many techniques have been reported, such as embedding FBG in polymer or Bonding FBGs on cantilever structure [15,16]. Hsu et al. developed a temperature compensated FBG based gas pressure sensor with a single FBG by applying an axial strain on it [17]. To compensate the temperature effect, they applied constructive stress on the sensor. Another group developed a depth sensor for under water remote operated vehicles (ROV), with temperature compensation and tested in lab by combining FBG with an optical Extrinsic Fabry-Perot Interferometer (EFPI) sensor [9]. A low-cost diaphragm based fiber bragg grating pressure sensor design for ocean applications has been presented and tested with different thickness of copper diaphragms [19].

In this paper, two designs for temperature compensated high-sensitive, low-cost and stable diaphragm based FBG pressure sensor are reported and discussed. Different types of metal diaphragms with varying

thickness were used for this study. Theoretical and experimental comparison for the best one has been carried out. The mechanical deformation of the diaphragm was calculated theoretically and validated through ANSYS finite element simulation software. The mathematical relationship between FBG wavelength and pressure applied has been reported. Also, by the diaphragm properties, the sensitivity was calculated by using MATLAB. Proposed sensor designs can capable to measure up to 300 meters depth of water with a resolution of 0.001 MPa, with linearity of 99.99% by using proper encapsulation methods and sealants. Proposed sensor design is easy to fabricate with low cost and low maintenance, also allows user to change the FBG on diaphragm with less effort. Samples are taken with the frequency of 25Hz which is equal to sensors response time of 40 milli seconds. Experiments were carried out for testing sensitivity and repeatability of both the sensor designs.

Sensor structure:

The FBG is a device commonly used in telecommunications technology and sensing. Fabricated by creating a periodic modulation of Refractive Index (RI) in the core of single mode (SM) fibre. Usually the FBG acts as a spectral filter such that, it reflects narrow band wavelength and transmits the remaining wavelengths, when the fibre is illuminated with a broad band source. The condition for the reflecting wavelength is showed in Eq. (1) and it is called Bragg's condition [1].

$$\lambda_B = 2n_{eff}\Lambda \quad (1)$$

Where n_{eff} is effective refractive index of grating in the fiber core, λ_B is central wavelength of the fiber grating, Λ is grating period. Here we used a standard telecommunication fiber (SMF-28) for all our experimentation [25,26]. When an external perturbation is applied on fiber there is change in core guided mode index is called effective refractive index of the fiber which is equal 1.44728 for SMF-28. The magnitude of refractive index change is 10^{-4} to 10^{-5} [27]. The effective refractive index is proportional to the concentration of the core dopant (mole% GeO_2) [28]. When an FBG is subjected to external perturbations both n_{eff} and Λ will change, which leads to shift in Bragg wavelength [29]. So, in response to change in strain, the total wavelength shift is given by [30]

$$\frac{\Delta\lambda_B}{\lambda_B} = 2n_{eff} \frac{\partial\Lambda}{\partial L} + 2\Lambda \frac{\partial n_{eff}}{\partial L} \quad (2)$$

$$\frac{\Delta\lambda_B}{\lambda_B} = \frac{1}{\Lambda} \frac{\partial\Lambda}{\partial L} \Delta L + \frac{1}{n_{eff}} \frac{\partial n_{eff}}{\partial L} \Delta L \quad (3)$$

The first term in the above Eq. (3) represents the strain of the grating period due to the extension of the fiber. Suppose we have a length L of a fiber with an inscribed FBG in it. If we apply a stress on the fiber of ΔL then we will have an relative strain $\frac{\Delta L}{L}$. At the same time if the FBG has a length L_{FBG} it will experience a strain $\frac{\Delta L_{FBG}}{L_{FBG}}$ but since the FBG is in the fiber, then $\frac{\Delta L_{FBG}}{L_{FBG}} = \frac{\Delta L}{L}$. Since the Bragg displacement with extension equals the displacement of the grating period with the same extension and, therefore, the first term in Eq. (3) is the unit.

The second term in Eq. (3) is the photo-elastic coefficient (P_e), the variation of the index of refraction with strain. When an extension is applied to the fiber, the two terms in Eq. (3) produce opposite effects, one by increasing the distance between gratings so that it will increase the wavelength and other by decreasing the refractive index change thus decreasing the Bragg wavelength. For a single mode fiber, central wavelength shift caused by strain and temperature change is given by Eq. (4) [2]

$$\frac{\Delta\lambda_B}{\lambda_B} = (1 - p_e)\Delta\epsilon + (\alpha_f + \xi)\Delta T \quad (4)$$

where p_e is the effective photo elastic coefficient of the fiber, is given by

$$p_e = \frac{n_{eff}^2}{2} [P_{12} - \mu(P_{11} + P_{21})] \quad (5)$$

P_{11} , P_{12} are photo elastic coefficients 0.121, 0.270 respectively, μ is Poisson's ratio value of 0.17, and by substituting n_{eff} values, we can obtain $p_e = 0.22$. $\Delta\epsilon$ is the strain change, α is thermal expansion coefficient of silica and ξ is thermo-optic coefficient of silica, and ΔT is the temperature variation. According to Eq. (4) the shift in wavelength varies linearly with both temperature and pressure. Here all experiments are done at constant room temperature so we neglected the second term in Eq. (4)

$$\Delta\lambda_B = \lambda_B(1 - p_e)\Delta\epsilon \quad (6)$$

From the above Eq. (6), wavelength shift due to effective refractive index is negligible, and therefore shift in wavelength is dominated by mechanical strain in the FBG when compare to effective refractive index change.

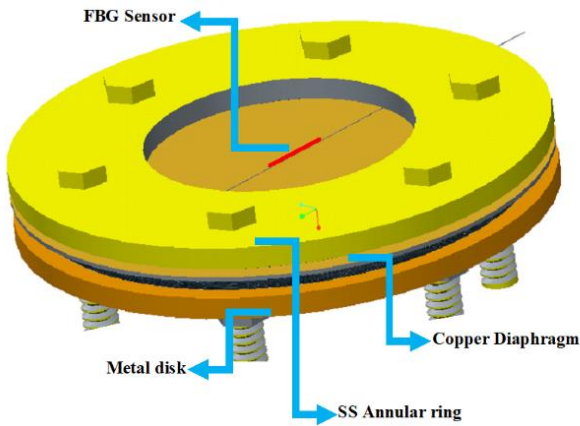


Fig:1 3D view of closed air cavity setup

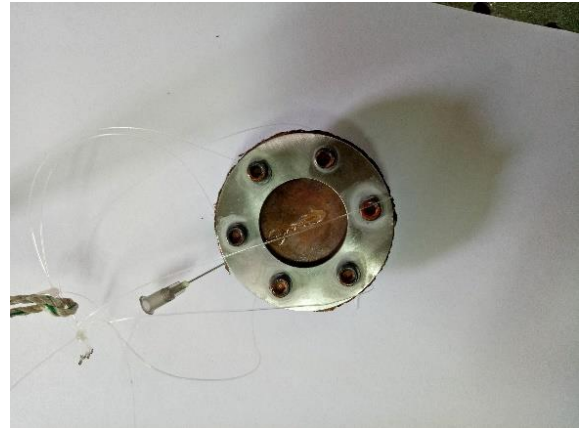


Fig:2 Closed air cavity sensor head

There are two models for the proposed FBG pressure sensor. One is the closed air cavity setup and, another one is the open-air cavity setup. 3D view of a closed air cavity setup is shown in Fig. 1, and experimental sensor head is shown in Fig. 2. This setup is made with a stainless steel annular ring with a thickness of 2.5 mm, copper diaphragm and a stainless steel disk with a thickness of 2.5 mm with a diameter of 60 mm. Annular ring and disk have four 'O' ring grooves to form a closed air cavity between diaphragm and disk, which reduces the pressure leakage. Here, the diaphragms are made with the copper sheet in circular shape with the diameter of 60 mm and thickness of 0.05 mm and 0.25 mm.

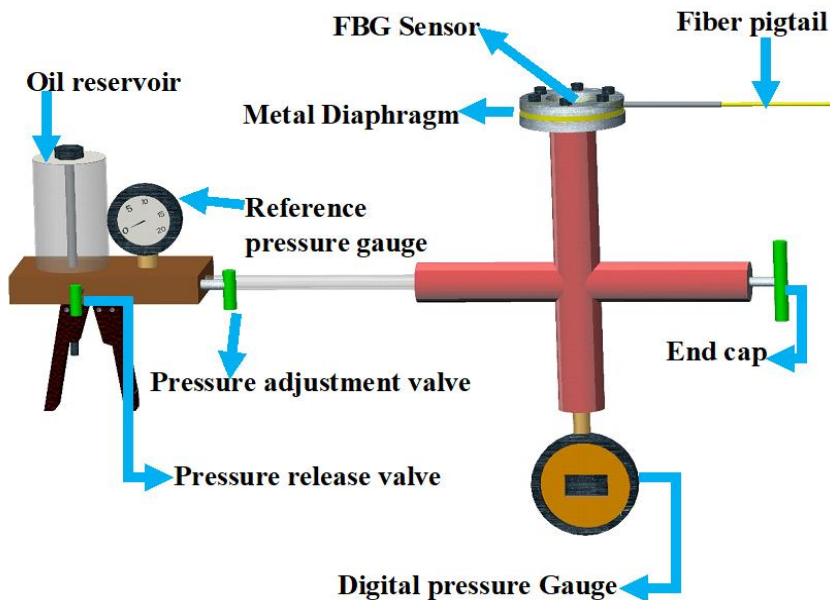


Fig: 3 Schematic 3D design of open-air cavity pressure measurement system

The schematic design of the open-air cavity setup is shown in Fig. 3. This has an oil-filled hand pump to create pressure inside the system and to apply on the diaphragm which creates positive pressure. By pressing plunger, oil is pushed from the reservoir through hosepipe and it is connected to a stainless-steel plus-shaped adapter with proper connectors. When pressure measurement is needed, system need to connect a reference

pressure gauge so the second port of the adapter is connected to a digital pressure gauge to measure the real-time pressure variations in the system. The third port is closed with an end cap to a pressure releasing mechanism. A stainless-steel disk 5 mm thick with a centre hole to pass the oil is welded on the fourth end of the connector. On top of welded stainless-steel disk, the diaphragms of copper and stainless-steel materials with different thickness are mounted. An annular ring with an inner diameter of 30 mm, the outer diameter of 60 mm and thickness of 3 mm, is fixed on metal diaphragms. The total system is now closed to maintain the pressure. By using fine adjustment screws in the system, pressure can be increased or decreased precisely. In both setups, FBG is fixed on top of the diaphragm with a cyano-acrylate glue, such that it is passing through the centre of the diaphragm. When pressure acts on the diaphragm, shape deformation takes place and strain develops in FBG which causes a wavelength shift proportional to pressure change. The diaphragm displacement and real-time variations is measured by using the ANSYS Finite Element simulation software. Deformation of the diaphragm is calculated theoretically by

$$D = \frac{qa^4}{64k} \quad (7)$$

Where D is the diaphragm deformation, q is applied pressure on diaphragm, a radius of the diaphragm, and k is the bending stiffness of the diaphragm.

$$k = \frac{Eh^3}{12(1 - \mu^2)} \quad (8)$$

E is Young's modulus of the diaphragm, μ is the Poisson's ratio of the diaphragm, and h is the diaphragm thickness.

As shown in Fig. 2,3 the spring element of the pressure sensor is a plane circular diaphragm, on which deformation or strain would be produced when liquid or gas pressure is applied. Based on small deformation theory [19], the radial strain ϵ_r and tangential strain ϵ_t on the diaphragm can be calculated by where p is the measured pressure, E is the Young's modulus of the plate, μ is the Poisson's ratio of shell, R is the radius of plate, r is the measuring distance from center, h is the diaphragm thickness. When pressure applied on the center of the diaphragm tangential strain will develop in it, which is equal to the axial strain of the FBG.

$$\epsilon_r = \frac{3(1 - \mu^2)(R^2 - 3r^2)}{8Eh^2} p \quad (9)$$

$$\epsilon_t = \frac{3(1 - \mu^2)(R^2 - r^2)}{8Eh^2} p \quad (10)$$

where p is the measured pressure, E is the Young's modulus of the plate, μ is the Poisson's ratio of shell, R is the radius of plate, r is the measuring distance from center, h is the diaphragm thickness. The tangential strain of the diaphragm can consider as the axial strain of the FBG

$$\epsilon_{t|r=0} = \epsilon_{axis} \quad (11)$$

$$\epsilon_t = \frac{\Delta l}{l} = \frac{3pR^2}{8Eh^2}(1 - \mu^2) \quad (12)$$

Where ϵ_{axis} is axial strain in FBG. The FBG strain sensitivity can be obtained from substituting equation (6) and (4) into (2). An FBG of central wavelength 1559nm, typical strain sensitivity is 0.001nm/ $\mu\epsilon$.

$$K = \frac{\Delta\lambda_B}{\lambda_B} = \frac{3\lambda_B R^2}{8Eh^2}(1 - \mu^2) \quad (13)$$

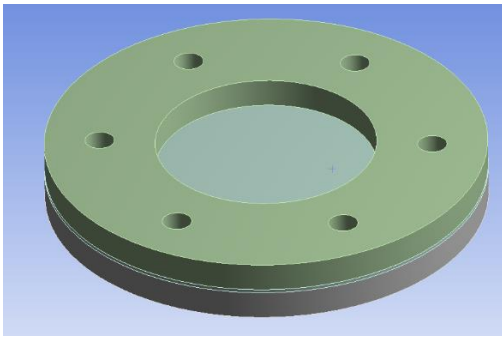
Where K is typical strain sensitivity of the sensor. From the Eq. (13) sensitivity of the sensor is depends on thickness and radius of a particular material.

Simulation analysis:

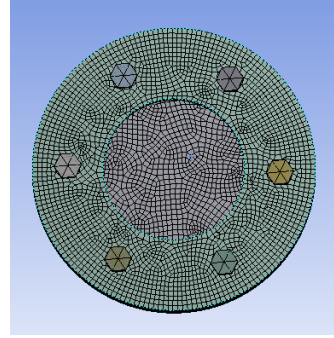
To validate the performance of the proposed FBG sensor models and to calculate the pressure sensitivity, simulation studies are performed. In our proposed models, metal diaphragm works as a pressure transducer. Different thickness of copper and 304-grade stainless steel are used as pressure transducers in the sensor design. The analysis is divided into two computational steps. In the first step need to create model of the sensor design and perform the global analysis on it. The result of the first step was used for the second, which gives a detailed analysis of the diaphragm deformation. The structure parameters of diaphragms are used in simulation and calculations are given in Table. 1. The solid model and global analysis of the sensor design in simulation software are shown in Fig. 4. The maximum deformation of the copper diaphragm with a thickness of 0.05 mm in closed air cavity with pressure variation of 0 to 0.04 MPa and in an open-air cavity with pressure variation of 0 to 0.1 MPa is shown in Fig. 5 (a) and (b). The detailed deformation values of the other diaphragms with different thicknesses under different pressure variations are given in Table. 2. The maximum displacement of the diaphragm takes place at the center, and it is decreased along the radius direction.

Table: 1 Structure parameters

S. N	Parameters	Copper material	Stainless-Steel material
1.	Young's modulus (E)	128 Gpa	200 Gpa
2.	Poisson's ratio (μ)	0.28	0.33
3.	Radius of the diaphragm (R)	15 (mm)	15 (mm)
4.	Thickness of material	0.05, 0.25, 0.5 (mm)	0.25, 0.5 (mm)

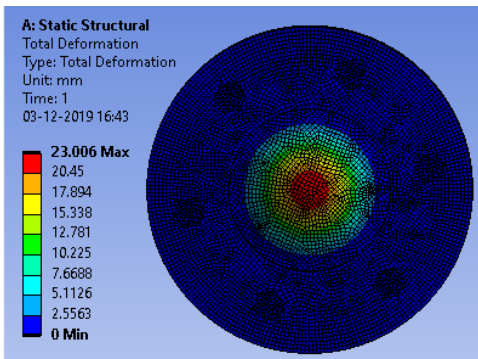


(a)

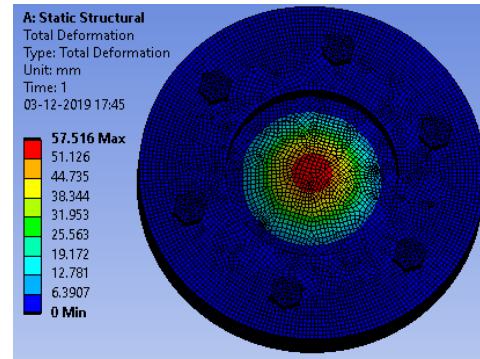


(b)

Fig: 4 ANSYS model of plates: (a) Solid model (b) Finite element model



(a)



(b)

Fig: 5 Results of ANSYS simulation (a) Displacement cloud of copper diaphragm with thickness of 0.05 mm under 0.04 Mpa (b) Displacement cloud of copper diaphragm with thickness of 0.05 mm under 0.1 Mpa.

S. No.	Thickness(mm)	Pressure (Mpa)	Material	Theoretical deformation (mm)	ANSYS deformation (mm)	Experimental deformation (mm)
1.	0.05	0.04	Copper	21.15	23.06	21.2
2.	0.05	0.1	Copper	52.87	57.51	53.1
3.	0.25	0.04	Copper	0.169	0.19	0.20
4.	0.25	0.5	Copper	2.114	2.405	2.2
5.	0.5	0.5	Copper	0.265	0.275	0.22
6.	0.25	0.5	Stainless Steel	1.352	1.411	1.39
7.	0.5	0.5	Stainless Steel	0.169	0.186	0.19

Table: 2 Diaphragm deformations

All parameters are measured in Millimetres (mm)

1. Experimental setup:

The schematic diagram of experimental setup is shown in Fig. 6. The agile, tunable broadband light source with a wavelength range 1528- 1568 nm allows interrogation at multi KHz frequencies with high accuracy 1 pm. A three port fiber optic circulator is connected with broad band source, sensor and optical interrogator. The light from broad band source is launched into the sensor via port1 of the optical circulator and the

reflected light from FBG sensor is sent to interrogator which is connected to port 3 via port 2. High precision and reliable Smartscan solid state FBG interrogator model is used as the optical interrogation system. This system has two channels for interrogation of FBGs, and in each channel, 16 FBGs can be interrogated simultaneously. This whole system works on wavelength division multiplexing (WDM).

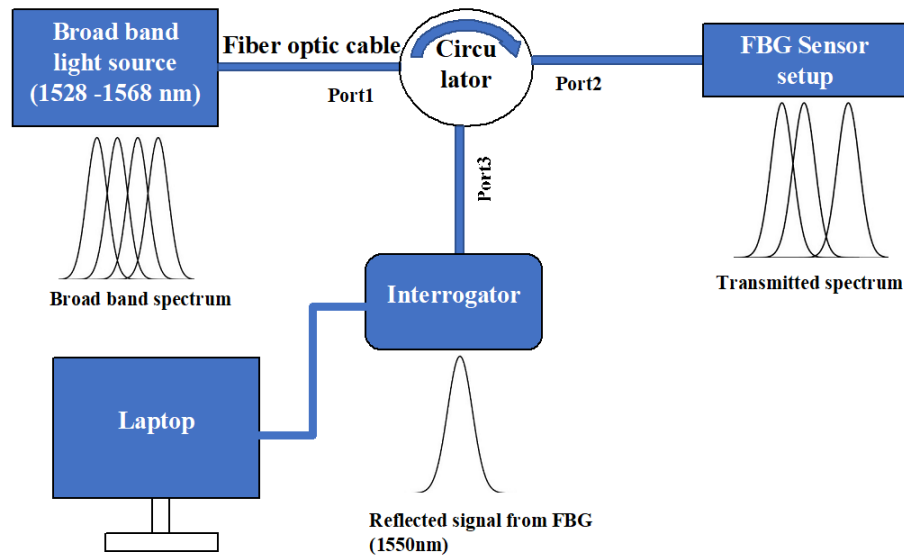


Fig: 6 Schematic diagrams of experimental setup

1.1 Closed air cavity pressure measurement setup

Closed air cavity pressure measurement setup is shown in Fig. 7. The sensor head is made with a metal diaphragm, metal disk, and rubber O rings. From bottom to top, first, we kept a metal disk with a thickness of 5 mm and a diameter of 60 mm. On top of the metal disk, we made two O ring grooves with a diameter of 50 mm and 45 mm. Second, a metal annular ring is made with an outer diameter of 60mm and an inner diameter of 30 mm, with a thickness of 3 mm kept on these two O rings. Third on top of the metal annular ring are made two O rings grooves with above-mentioned dimensions. A metal diaphragm is attached above these O rings so that a closed air cavity will form between metal disk and diaphragm. The depth of the cavity is equal to the thickness of the annular ring. On top of the diaphragm, one more annular ring with the same dimensions as above is attached. An acrylic-coated 10mm long FBG sensor with central wavelength 1549.65 nm is pasted on metal diaphragm along the diameter with cyanoacrylate glue. When assembled this there is an air trapped between diaphragm and metal disk so that it forms a closed air cavity. We have dipped this total setup in a 4-meter water tank for pressure measurements. Top view of the sensor head is shown in Fig. 8(a), and when pressure acts on a diaphragm, it will deform in a downward direction, as shown in Fig. 8(b). The FBG's fiber pigtail is connected to optical interrogator by using FC/APC connector and the interrogator is connected to the computer by network cable to see the reflected spectrum from sensor. Smartsoft software is used for the

spectrum analysis. By using this software, frequency of data acquisition can be varied from 1-25 kHz. The sensor head is moved vertically three times in water column and pressure is measured at an interval of 10 cm from 0 to 4 meters depth. The temperature of the water is measured at (27°C).

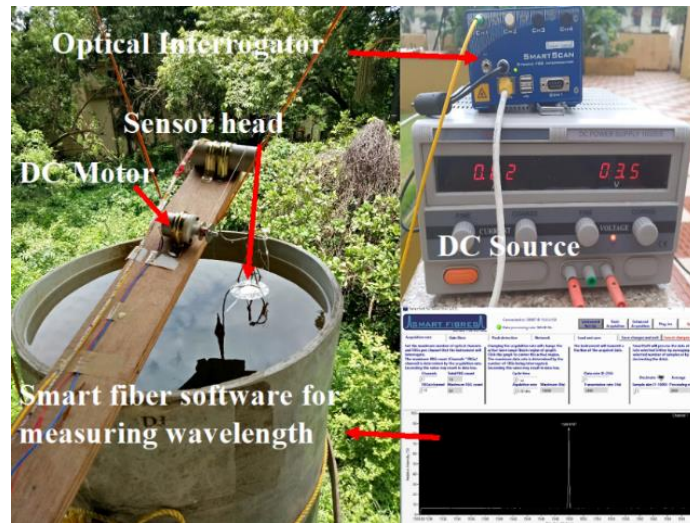


Fig. 7 Closed air cavity pressure measurement setup

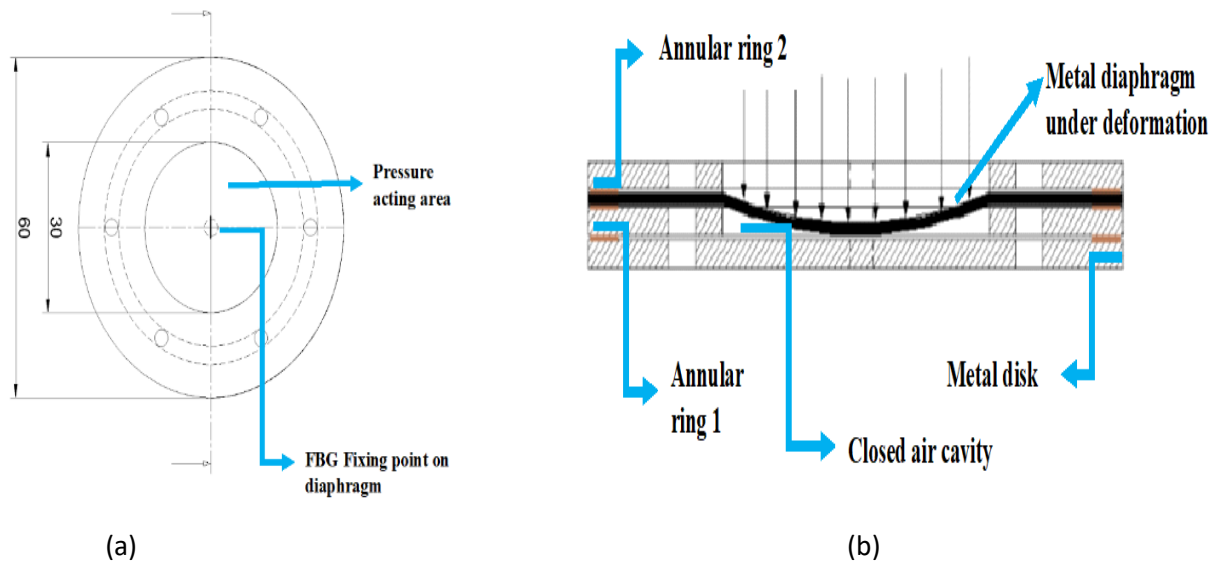


Fig: 8 Closed air cavity sensor head (a) Top view, (b) Front view

1.2 Open-air cavity pressure measurement setup:

The schematic 3D-design for an open-air cavity pressure measuring system is shown in Fig. 3 and the experimental configuration is shown in Fig. 9. Open-air cavity setup has an oil pump with a reference pressure gauge to know the applied pressure and a plunger to apply the pressure manually on the diaphragm. Two stainless steel tubes of 304 grade are cross welded in "+" shape. The first end of the tubes is connected to an oil pump with a flexible rubber tube and suitable connectors to reduce the oil leakage. The second end is

connected with a Keller digital manometer with model number LEO 1 is a microprocessor-controlled, accurate and versatile digital pressure measuring system, which is capable of measuring 300 bar pressure with 0.1 bar resolution. The third end is closed by an end cap to restrict oil leakage and also can be used as a pressure release valve. A stainless-steel disk with a thickness of 5 mm, and diameter of 60 mm is mounted and welded on the fourth end. On top of the Stainless-steel disk we made an O ring groove with 50 mm diameter. Above this O ring, a metal diaphragm with different thicknesses (0.05,0.25,0.5 mm) and diameter of 60 mm is kept. On top of the diaphragm, an annular metal ring with an outer diameter of 60 mm and an inner diameter of 30 mm with a thickness of 3 mm is placed. Finally, the diaphragm is sandwiched between mounted disk and annular ring by using nuts and bolts. Top view of the sensor head is shown in Fig. 10(a)

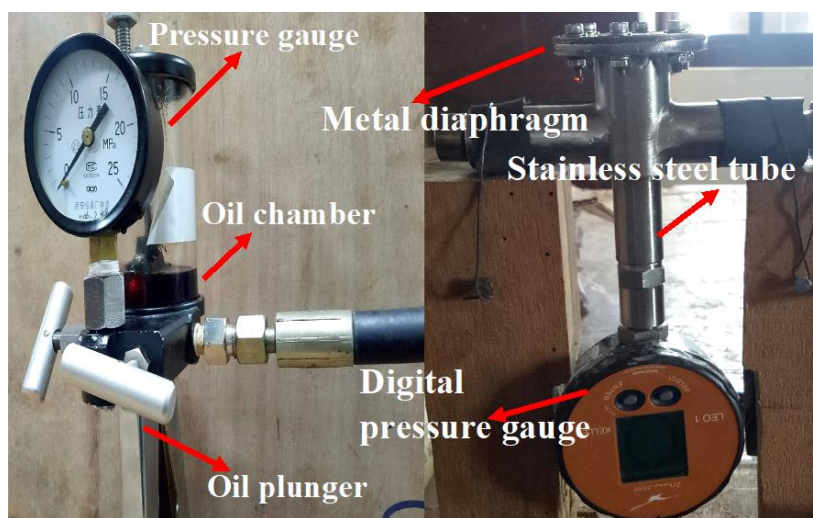


Fig: 9 Open-air cavity pressure measurement setup

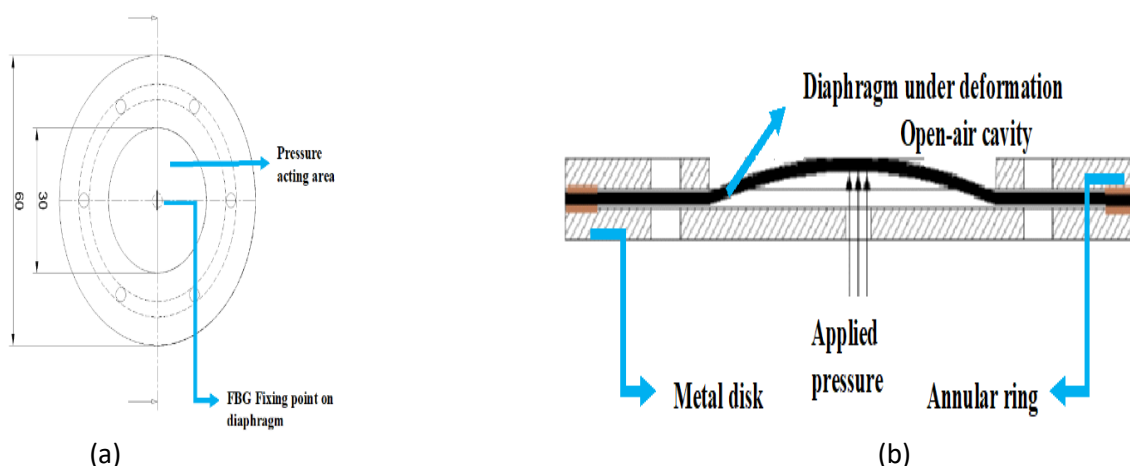


Fig: 10 Open-air cavity sensor head (a) Top view, (b) Front view

By pressing the plunger, oil travels from the reservoir through the hosepipe, and it will reach to stainless steel tubes so that the pressure inside the system at every point is identical since all four ends of the Stainless-

steel tubes are closed, and there is no chance of oil leakage. So oil pressure acts on the diaphragm. Due to this, deformation takes place at the center of the diaphragm in positive Z-direction such that diaphragm is on XY plane towards open-air through the annular ring inner diameter and it acts as an open-air cavity. The deformed shape of the diaphragm is showed in Fig. 10(b). At the same time, the digital pressure gauge shows the real-time pressure of the system. The pressure is raised from 0 - 0.5 MPa with an interval of 0.01 MPa, and the temperature of the measuring system is at room temperature 27°C. Due to deformation of the diaphragm, a lateral strain in the FBG is caused, and the wavelength shift in the FBG sensor is recorded for each interval of pressure.

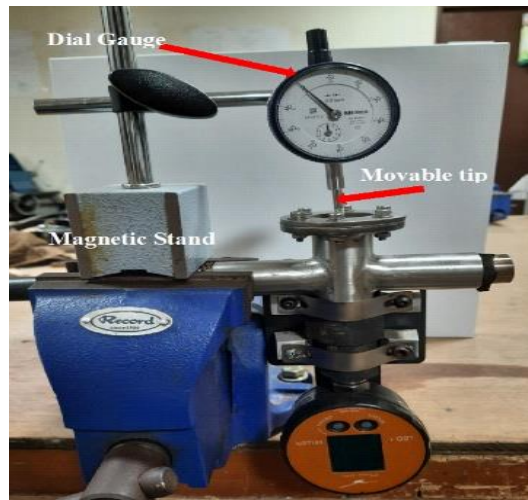


Fig: 11 Diaphragm deformation with dial gauge

The real time diaphragm deformations are measured in open-air cavity setup by using a Mitutoyo dial indicator attached with magnetic stand. The round scale in this indicator is able to adjust zero reading after each measurement cycle so that error in measurement is negligible and it can measure maximum deformation of diaphragm up to 10 cm with the resolution of 0.01 mm. Before applying pressure, the tip of indicator is need to attach the diaphragm surface so that it will show some reading in indicator scale and that reading need to adjust to zero by rotating entire circular scale. When pressure acting on diaphragm, deformation occurs and it causes the tip displacement in vertically upward direction. The experimental setup is shown in Fig. 11.

2. Results and Discussions:

5.1 Closed air cavity results:

In closed air cavity method, to check the repeatability and performance of sensor the sensor-head was descended and ascended in a 4 meters deep water tank. In both Open and Closed air cavity sensor measurements are done with 25Hz frequency. Fig. 12 shows wavelength shift with pressure variation

measured by using a copper diaphragm with a thickness of 0.25 mm. Pressure sensitivity from the slope of the curve is 0.2286 nm/MPa and linearity of 96.29% is observed. The results are showed less repeatability, low sensitivity and experimental values deviated from theoretical curve, this may cause due to the fixing position of sensor on the diaphragm or deformation of diaphragm is not linear with pressure. To increase the pressure sensitivity and linearity of the sensor, the thickness of copper plate is reduced to 0.05 mm. The pressure variation with wavelength shift is shown in Fig. 13. The pressure sensitivity is 24.59 nm/MPa, and the linearity of 99.72% is observed. To test for higher pressure range, the open-air cavity technique is adopted.

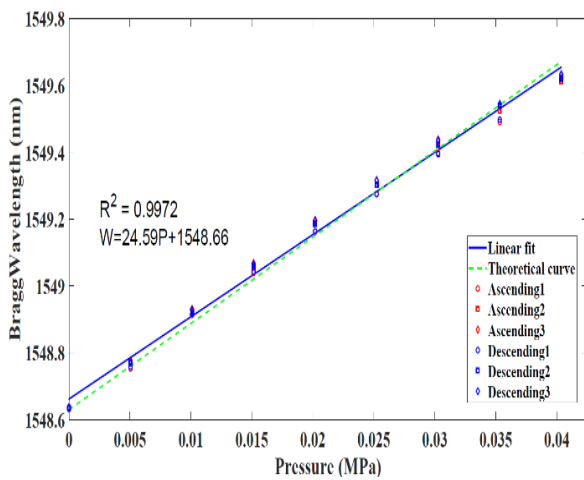


Fig: 12 Wavelength shift with pressure measured by 0.25 mm thickness of copper plate by closed air cavity setup.

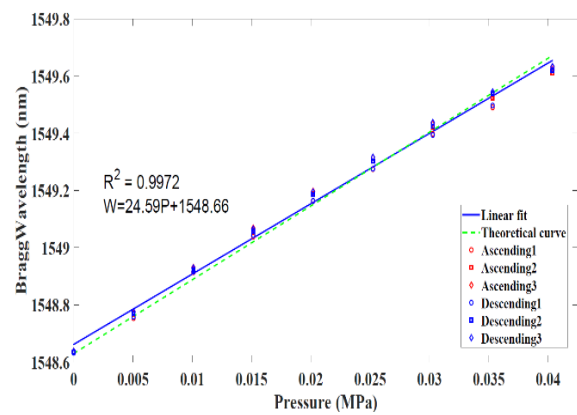


Fig: 13 Wavelength shift with pressure measured by 0.05 mm thickness of copper plate by closed air cavity setup.

5.2 Open-air cavity results:

In the open-air cavity setup, the range of pressure measurement can be increased by 10 times more than closed air cavity setup. Different thicknesses of copper and stainless steel diaphragms are tested. Repeatability of sensor is tested for three times with each diaphragm by increasing and decreasing the pressure from 0 to 5 MPa. Theoretical results are plotted with experimental results for each experiment. Copper diaphragm with thickness of 0.25 mm is tested under the pressure range from 0 - 0.5 MPa. Fig. 14 shows the wavelength shift with pressure variation and the pressure sensitivity is calculated as 5.6097 nm/MPa with linearity of 99.64%. Fig. 15 shows the wavelength shift variation with pressure by a copper diaphragm of thickness 0.05 mm. Pressure sensitivity measured with this diaphragm is 16.22 nm/MPa which is higher compared with 0.25 mm thickness plate. Here the pressure range is measured up to 0.1 MPa due to the lesser thickness of diaphragm. Further, different thickness's of copper and stainless steel diaphragms are tested for more sensor stability and

linearity in 300 meters depth of the ocean. Fig. 16 shows the wavelength shift with pressure measured by using open-air cavity with thickness of 0.5 mm copper diaphragm, observed sensitivity is 2.7802 nm/MPa which is two times more than reported in [20] with linearity of 99.89%. Fig. 17 shows the wavelength shift with pressure variation using 0.25 mm stainless steel plate with the sensitivity of 2.63 nm/MPa and linearity of 99.83%. Fig. 18 shows the wavelength shift variation of FBG with pressure measured by open-air cavity setup and with 0.5 mm stainless steel plate. With the linearity of 99.79%, the sensitivity of the sensor is 1.305 nm/MPa (10 times more with double shell cylinder measurement) [23]. Fig. 19 shows theoretical sensitivity with diaphragm thickness. From this one can able to choose the diaphragm with thickness for particular range of applications. Also shows that our experimental results are followed the theoretical curves. Theoretical results can be matched with experimental ones by setting up the FBG at $\frac{R}{\sqrt{3}}$ location on the plate and need to be consider exact mechanical properties of the plate, where R is radius of diaphragm. Table. 3 shows the experimental results of the proposed sensor designs.

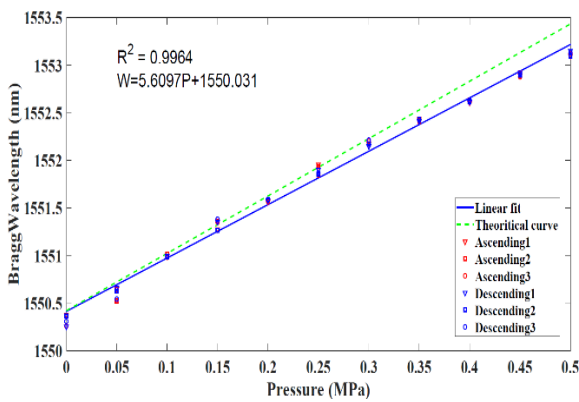


Fig: 14 Wavelength shift with pressure measured by 0.25 mm thickness of copper plate by open-air cavity setup.

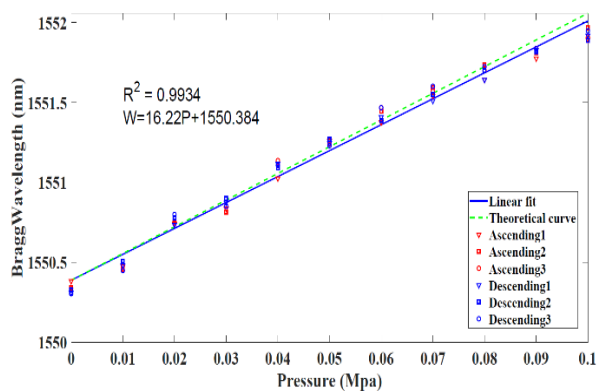


Fig: 15 Wavelength shift with pressure measured by 0.05 mm thickness of copper plate by open-air cavity setup.

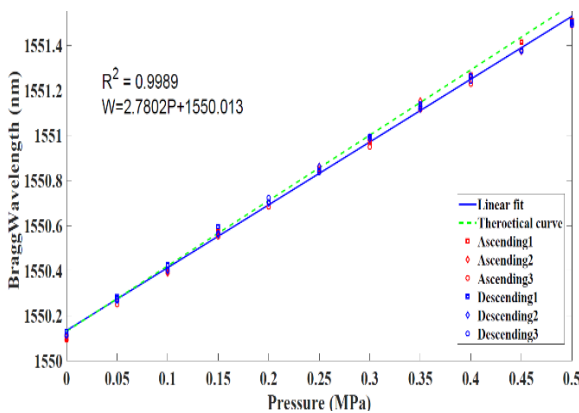


Fig: 16 Wavelength shift with pressure measured by 0.5 mm thickness of copper plate by open-air cavity setup.

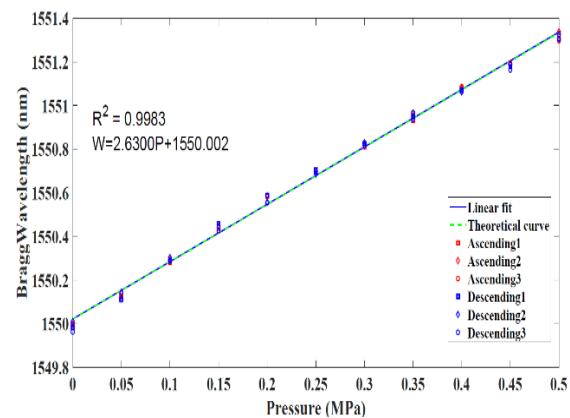


Fig: 17 Wavelength shift with pressure measured by 0.25 mm thickness of stainless steel plate by open-air cavity setup.

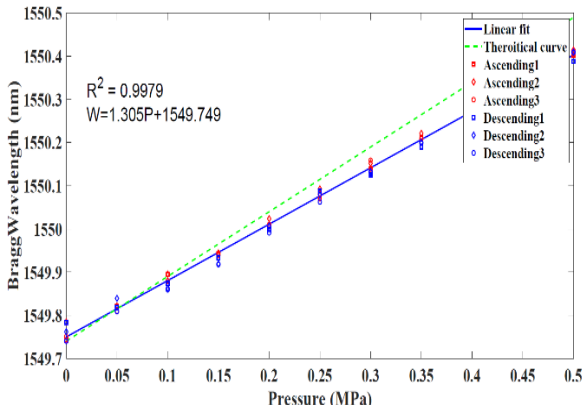


Fig: 18 Wavelength shift with pressure measured by 0.5 mm thickness of stainless

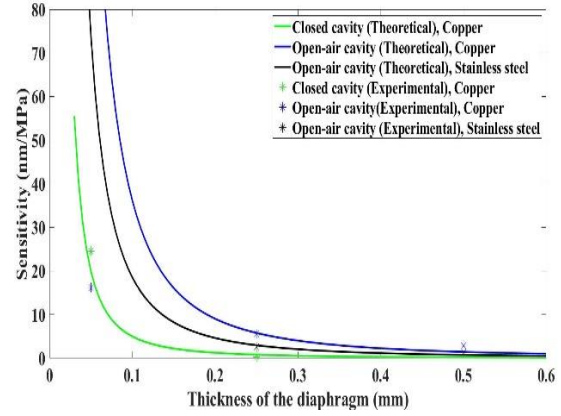


Fig: 19 Sensitivity variation with diaphragm thickness.

Table: 3 Experimental results of the proposed sensor design

S. No.	Type of setup	Material	Thickness (mm)	Sensitivity (nm/Mpa)	Linearity (%)
1.	Closed air cavity	Copper	0.05	24.59	99.72
2.	Closed air cavity	Copper	0.25	0.2286	96.29
3.	Open-air cavity	Copper	0.05	16.22	99.34
4.	Open-air cavity	Copper	0.25	5.458	99.17
5.	Open-air cavity	Copper	0.5	2.7802	99.89
6.	Open-air cavity	Stainless-steel	0.25	2.6300	99.83
7.	Open-air cavity	Stainless-steel	0.5	1.305	99.79

3. Conclusions:

Pressure measurements with different thickness of stainless steel and copper diaphragms with bare FBG are studied. The sensitivity of the sensor is tested with two different designs and with different metal diaphragms as pressure transducer. Results are indicating that the copper plate with 0.05 mm thickness is more sensitive and linear. In closed air cavity system, maximum pressure sensitivity of 24.59 nm/MPa is achieved and in the open-air cavity setup, maximum pressure sensitivity of 16.22 nm/MPa is achieved. Closed and open-air cavity linearities are observed to be 99.72% and 99.34% respectively. From the above analysis, suitable diaphragm can be chosen very easily for particular pressure range. An extended work is ongoing for the temperature compensation of sensor while measuring the pressure, by using single FBG and to enhance the sensitivity of sensor and for measuring temperature and pressure simultaneously in actual fields of ocean.

4. **Acknowledgement:**

Authors would like to thank Prof. Balaji Srinivasn, Prof. in Department of Electrical Eng. IIT Madras for providing FBG sensors.

5. **Author's Contribution statement:**

All the authors were involved in the theoretical analysis and experimental studies of the manuscript. Also all the authors have read and approved the final manuscript.

References:

1. L. A. Rutterford, "Future fish distributions constrained by depth in warming seas," *Nat. Clim. Change* **5**, 569, (2015).
2. S. J. Mihailov, "Fiber Bragg grating sensors," *Sensors* **12**(2) 1898--1918 (2012).
3. D. A. Krohn, T. MacDougall, and A. Mendez, "Fiber optic sensors: fundamentals and applications," Spie Press Bellingham, WA (2014).
4. Y. J. Rao, "Recent progress in in-fiber bragg grating sensors: applications," in *Proc. SPIE*, **3555**, 429--442 (1998).
5. G. Constantin, G. Perrone, S. Abrate, et al., "Fabrication and characterization of low-cost polarimetric fiber-optic pressure sensor," *J. Optoelectron. Adv. M.* **8**(4), 1635 (2006).
6. S. H. Aref, H. Latifi, M. I. Zibaii, et al., "Fiber optic fabry-perot pressure sensor with low sensitivity to temperature changes for downhole application," *Opt. Commun.* **269**(2), 322--330 (2007).
7. P. Vengal~Rao, K. Srimannarayana, M. Sai Shankar, et al., "A diaphragm based low-cost fiber optic pressure sensor," *Microw Opt Technol Lett.* **54**(10), 2229--2231 (2012).
8. K. O. Hill and G. Meltz, "Fiber bragg grating technology fundamentals and overview," *J. Lightwave Technol.* **15**(8), 1263--1276 (1997).
9. D. Duraibabu, G. Leen, D. Toal, et al., "Underwater depth and temperature sensing based on fiber optic technology for marine and fresh water applications," *Sensors* **17**(6), 1228 (2017).
10. P. S. Reddy, R. L. N. S. Prasad, D. S. Gupta, et al., "Encapsulated fiber bragg grating sensor for high temperature measurements," *Opt. Eng.* **50**(11), 114401 (2011).
11. J. Xu, G. Pickrell, B. Yu, et al., "Epoxy-free high-temperature fiber optic pressure sensors for gas turbine engine applications," in *Proc. SPIE*, **5590**, 1--10 (2004).
12. G. Allwood, G. Wild, A. Lubansky, et al., "A highly sensitive fiber bragg grating diaphragm pressure transducer," *Opt. Fiber Technol.* **25**, 25--32 (2015).
13. F. Urban, J. Kadlec, R. Vlach, et al., "Design of a pressure sensor based on optical fiber bragg grating lateral deformation," *Sensors* **10**(12), 11212--11225 (2010).
14. J. Huang, Z. Zhou, X. Wen, et al., "A diaphragm-type fiber bragg grating pressure sensor with temperature compensation," *Measurement* **46**(3), 1041--1046 (2013).
15. H. Ahmad, S. W. Harun, W. Y. Chong, et al., "High-sensitivity pressure sensor using a polymer-embedded fbg," *Microw Opt Technol Lett.* **50**(1), 60--61 (2008).
16. S. Pevec and D. Donlagi'c, "Multiparameter fiber-optic sensors: a review," *Opt. Eng.* **58**(7), 072009 (2019).
17. Y. Hsu, L. Wang, W.-F. Liu, et al., "Temperature compensation of optical fiber bragg grating pressure sensor," *IEEE Photon. Technol. Lett.* **18**(7), 874--876 (2006).

18. V. V. S. C. Swamy, P. S. Reddy, V. P. Vijeesh, et al., "A diaphragm based fiber bragg grating (fbg) type pressure sensor for ocean applications," in *Proc. SPIE*, **11088**, 77--84 (2019).
19. S. P. Timoshenko and S. Woinowsky-Krieger, *Theory of plates and shells*, McGraw-hill (1959).
20. H. Ahmad, W. Y. Chong, K. Tambiratnam, et al., "High sensitivity fiber Bragg grating pressure sensor using thin metal diaphragm," *IEEE Sensors J.*, **9**(12), 1654--1659 (2009).
21. C. Wu, Y. Zhang, and Bai-Ou Guan, "Simultaneous measurement of temperature and hydrostatic pressure using Bragg gratings in standard and grapefruit microstructured fibers," *IEEE Sensors J.*, **11**(2), 489--492 (2010).
22. J. Huang, Z. Zhou and Y. Tan et al., "Design and experimental study of a Fiber Bragg grating pressure sensor," in *Proc. IEEE*, 217--221 (2014).
23. Wento, Z., F. Li, Y. Liu, et al., "FBG pressure sensor based on the double shell cylinder with temperature compensation," *Measurement*, **42**(3), 408-411 (2009).
24. Rao, Y. J., et al., "Temperature-strain discrimination using a wavelength-division-multiplexed chirped in-fibre-Bragg-grating/extrinsic Fabry-Perot sensor system," in *Chin. Phys. Lett.*, **18**(643) (2001).
25. Juelich, Florian, and Johannes Roths. "OP2-determination of the effective refractive index of various single mode fibres for fibre Bragg grating sensor applications," in *Proc. OPTO*, 119-124 (2009).
26. Kashyap, R., "Fiber bragg gratings," Academic press, (2009).
27. Wen, K., Peng, H., et al., "Finite element analysis of a novel weak-pressure sensor based on fiber Bragg gratings in photonic crystal fibers," in *Opt. Eng.* **48**(3), 34402 (2009).
28. Gruner-Nielsen, L and Hubner, J, "Photosensitive fiber for highly reflective Bragg gratings," in *Proc. IEEE*, 178-179 (1997).
29. Xu, M.G., Reekie, L., et al., "Optical in-fibre grating high pressure sensor," in *Electronics lett.*, **29** (4), 398--399 (1993).